ELSEVIER

Journal of Fluids and Structures 22 (2006) 793–806

JOURNAL OF FLUIDS AND STRUCTURES

www.elsevier.com/locate/jfs

Wake transition of two-dimensional cylinders and axisymmetric bluff bodies

M.C. Thompson*, K. Hourigan, K. Ryan, G.J. Sheard

Fluids Laboratory for Aeronautical and Industrial Engineering (FLAIR), Department of Mechanical Engineering, PO Box 31, Monash University, Clayton, 3800, Vic., Australia

Received 28 April 2006; accepted 11 May 2006
Available online 24 July 2006

Abstract

This article presents a short review of the three-dimensional transition of wakes from two-dimensional bodies, such as cylinders of various cross-sectional shape, and axisymmetric tori or rings. The nature and sequence of instabilities are compared and contrasted, especially with reference to the base case of the circular cylinder wake. The latter has been the subject of intense interest and scrutiny for well over a century, and has implicitly assumed the role of providing the generic transition scenario for turbulent wake flow. For elongated cylinders with streamlined leading edges, the analogues of the instability modes for a circular cylinder become unstable in the reverse order, which may have implications for the route to wake turbulence for such bodies. As well, the analogue of mode B has a significantly increased relative spanwise wavelength and appears to have a different near-wake structure. At the other extreme, for a normal flat plate, the wake first becomes unstable to a nonperiodic mode that appears distinct from either of the dominant circular cylinder wake modes. For tori, which have a local geometry approaching a two-dimensional circular cylinder for high aspect ratios (ARs), the sequence of transitions with increasing Reynolds number is a strong function of AR. For intermediate ARs, the first occurring wake instability mode is a subharmonic mode. Possible underlying physical mechanisms leading to some of these instabilities are also examined. In particular, support is provided for the role of idealized physical instability mechanisms in controlling wavelength selection and amplification for the dominant wake instability modes. The results presented in this article focus on relevant research undertaken by the Monash group but draws in results from many other international groups.

1. Introduction

Considerable experimental and computational effort has gone into documenting the three-dimensional wake transitions of a nominally two-dimensional circular cylinder. A nonexhaustive but representative sample of articles includes Williamson (1988b, 1996a,b), Wu et al. (1996), Thompson et al. (1994, 1996), Barkley and Henderson (1996), Henderson (1997), Mittal and Balachandar (1995), Karniadakis and Triantafyllou (1992), Brede et al. (1996), Bays-Muchmore and Ahmed (1993), and Gerrard (1978). Stability analysis (Barkley and Henderson, 1996) indicates that the two-dimensional wake becomes linearly unstable to mode A at $Re \simeq 190$, and the base flow undergoes a further bifurcation to mode B at $Re \simeq 260$. Experiments (Williamson, 1988b; Miller and Williamson, 1994) and direct

*Corresponding author. Tel.: +61 3 9905 9645; fax: +61 3 9905 9639.
E-mail address: mark.thompson@eng.monash.edu.au (M.C. Thompson).

0889-9746/$ - see front matter © 2006 Elsevier Ltd. All rights reserved.
doi:10.1016/j.jfluidstructs.2006.05.001

numerical simulations (DNS) (Thompson et al., 1996; Henderson, 1997) show that mode B becomes unstable at a significantly lower Reynolds number ($Re = 230-240$). At slightly higher Reynolds numbers, there is a strong nonlinear interaction between the modes and the wake undergoes a rapid transition to spatio-temporal chaos (Henderson, 1997), so that it is effectively turbulent for a Reynolds number of just a few hundred. The growth and saturation of the modes in the wake have been modelled in detail using the Landau equation (Henderson, 1997; Sheard et al., 2003a). Finally, the underlying physical mechanism driving the instability modes has been explored by various authors, including Barkley and Henderson (1996), Henderson (1997), Leweke and Williamson (1998b), and Thompson et al. (2001b). Fig. 1 shows a side-by-side comparison of experimental and numerical tracer visualizations of the mode A and B shedding modes. Thus it appears that this wake has been well documented and is well understood; however, an obvious question is whether this transition scenario is generic or universal for a variety of other two-dimensional and axisymmetric body shapes. This question is addressed by the current paper.

The FLAIR (Fluids Laboratory for Aeronautical and Industrial Research) group at Monash University has spent some effort investigating the effect of body shape on wake transition. In particular, two broadly representative families

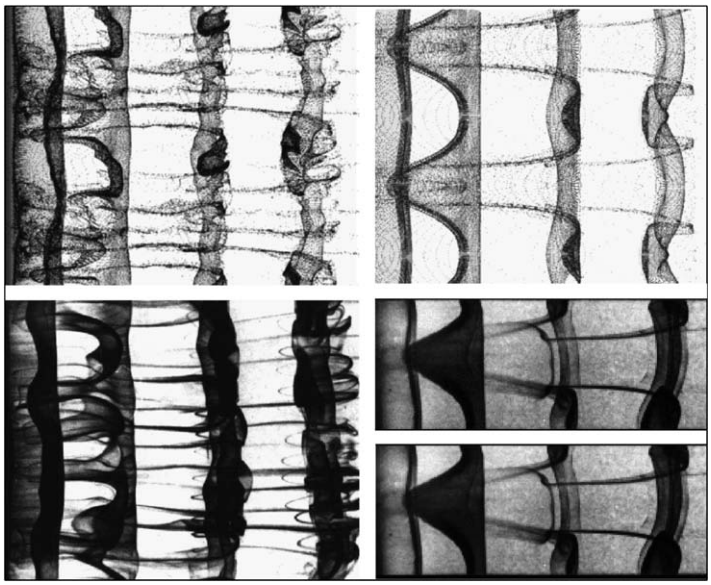

Fig. 1. Numerical visualizations of the two shedding modes using passive tracer particles (top) compared with experimental dye visualizations obtained by Williamson (199a,b). Mode B is shown at the left and mode A at the right.

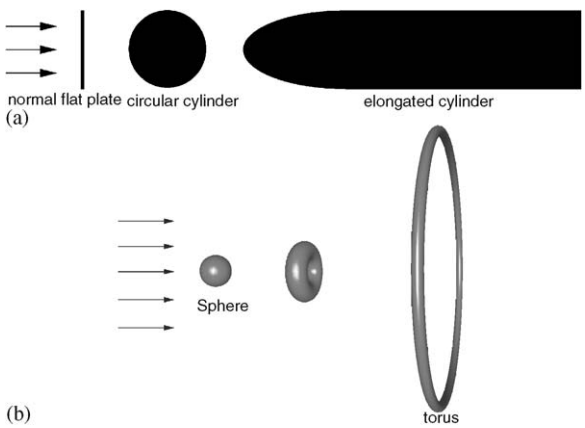

Fig. 2. Top: sequence of (cross-sections of) two-dimensional cylinders used to study two-dimensional wake evolution. Bottom: axisymmetric bodies examined.

of body geometry have been examined, which include previously well-studied generic body shapes as limiting cases. The first set consists of the normal flat plate, a circular cylinder, and elongated cylinders with elliptical-leading edges to prevent vortex shedding except from the trailing edge. The second set focusses on axisymmetric bodies, in particular a ring or torus placed with its axis aligned with the flow direction. By adjusting the AR, this topology can be transformed continuously from a sphere to a very large ring where curvature effects are negligible, so that a section of the geometry is representative of a circular cylinder. These sequences of body shapes are depicted in Figs. 2(a) and (b).

2. Wake transition of two-dimensional bodies

Table 1 provides an overview of the cases considered in this section. The critical Reynolds numbers, wake mode descriptions and the preferred wavelengths are given for circular and square cylinders, the normal flat plate, and an elongated streamlined leading-edge blunt trailing-edge cylinder. References to the original sources are provided in the following subsections.

2.1. Circular and square cylinders

As mentioned above, the three-dimensional transitions in the wake of a circular cylinder have been extensively studied experimentally, numerically and theoretically. The wake becomes unstable to three-dimensional perturbations through a subcritical (i.e., hysteretic) transition (Henderson, 1997) to an instability mode, dubbed mode A by Williamson (1988a) [also see Williamson (1996a,b)], at $\mathrm{Re} \simeq 190$. The wavelength of this mode is approximately $4D$, where D is the cylinder diameter. Experimentally it is found that the saturated mode is not periodic, at least for Reynolds numbers not too far in excess of transition. DNS at $\mathrm{Re} = 210$, have confirmed this behaviour [Sheard, private communication; also see Henderson (1997)]. The reason for the loss of periodicity as the mode reaches saturation is still unclear. Floquet stability analysis (Barkley and Henderson, 1996) of the two-dimensional base flow indicates that a second mode, known as mode B, becomes unstable at $\mathrm{Re} \simeq 260$. This has a much shorter preferred wavelength of $\lambda/D \simeq 0.8$ and is unstable over a relatively narrow wavelength range. In experiments and DNS this mode is seen at much lower Reynolds numbers, $\mathrm{Re} \gtrsim 230$, presumably due to the modification of the two-dimensional wake by the saturated mode A state. The wake becomes chaotic rapidly with increasing Reynolds number through spatio-temporal chaos (Henderson, 1997), and is effectively turbulent at $\mathrm{Re} \gtrsim 300$. Importantly, the wake continues to show strong evidence of the mode B wavelength at much higher Reynolds numbers (Wu et al., 1996). The associated structures presumably contribute significantly to lateral mixing, and may be the dominant source at least in the near wake, even in the strongly turbulent case.

Two other instability modes have been found for the circular cylinder wake. The first of these is known as mode C (Zhang et al., 1995). This mode is artificially generated by perturbing the flow on one side of the wake. This leads to a subharmonic mode of intermediate spanwise wavelength between those of mode A and mode B. Studies of a square cylinder Robichaux et al. (1999), see below, also revealed mode S (for subharmonic). This mode also exists for a circular cylinder wake, and evidence for it in the subcritical state was provided by Barkley and Henderson (1996). Blackburn et al. (2005) provide accurate estimates of the critical Reynolds number and corresponding wavelength given in Table 1. This mode is not subharmonic, although it has a period close to two base periods, hence the designation of mode S was relabelled to mode QP (quasi-periodic) by Blackburn et al. (2005). The onset Reynolds number is considerably higher than the two better known modes and it is unlikely that it plays a role in wake transition, since the wake is highly nonlinear and demonstrates spatio-temporal chaos at considerably lower Reynolds numbers (Henderson, 1997).

Robichaux et al. (1999) performed a Floquet stability analysis of the wake of a square cylinder. The transition scenario appears to be similar to the circular cylinder. Again, modes A and B occur in the same sequence with transition Reynolds numbers of about 160 and 190, respectively. The maximally amplified wavelengths are also similar at 1.2 and 5.5 times the cylinder height. Interestingly, if the scale length is taken as the length of the diagonal, the preferred wavelengths are the same as for the circular cylinder to within a few percent. These authors also found a further instability mode, mentioned above, called mode S, which occurred at a higher critical Reynolds number of $\mathrm{Re} = 200$, and has a wavelength between mode A and mode B wavelengths. Blackburn and Lopez (2003) subsequently showed that, in fact, this mode was not a subharmonic, but was a mode with a complex Floquet multiplier with a period of only approximately twice the base flow period. A theoretical analysis based on symmetry groups (Blackburn et al., 2005) of the possible modes for geometries with this set of flow symmetries, indicated the only modes with the time–space symmetries of modes A and B could occur. The occurrence of a true subharmonic mode would be extremely unlikely.

Table 1
Transition behaviour for a series of different two-dimensional cylinders

Geometry	Geometry change relative to the circular cylinder	First instability	Second instability	Third instability	Comments
Circular cylinder	Standard case—diameter D	Mode A, $Re_c = 189$, $\lambda = 3.96D$, subcritical	Mode B, $Re_c = 259$, $\lambda = 0.82D$, supercritical	Mode QP, $Re_c = 377$, $\lambda \cong 2D$, quasi-periodic	Saturated state has Mode B wavelength/structure at much higher Re
Square cylinder	Sharp leading and trailing edges—two shedding points from each half, width $= D$	Mode A, $Re_c = 162$, $\lambda = 5.2D$	Mode B, $Re_c = 190$, $\lambda = 1.2D$, supercritical	Mode S, $Re_c = 200$, $\lambda = 2.8D$, almost subharmonic	Mode wavelengths similar to a circular cylinder if diagonal length used as scaling parameter
Normal flat plate	Shortened cylinder, height H	Quasiperiodic Mode, $Re \cong 105-110$, $\lambda \cong 5-6D$	Mode A, $Re_c \cong 125$, $\lambda \cong 2D$		First unstable model is a quasi-periodic mode
Elliptical leading-edge cylinder	Elongated cylinder, height H				
Aspect ratio: 2.5	Slight increase in afterbody length	Mode A, $Re_c \cong 240$, $\lambda \cong 7H$ reducing to quickly about $4H$			Elliptical leading edge causes flow to remain attached until separation from the trailing edge
Aspect ratio: 7.5		Mode B′, close to neutrally stable for $400 < Re < 500$, $\lambda \cong 2.2H$	Mode A, $Re_c \cong 470$, $\lambda \cong 3.9H$		Mode B′ is similar to mode B in overall spatio-temporal symmetry, but wavelength much larger
Aspect ratio: 12.5		Mode B′, $Re_c \cong 410$, $\lambda \cong 2.2H$	Mode A, $Re_c \cong 610$, $\lambda \cong 4H$		
Aspect ratio: 17.5	Very long cylinder	Mode B′, $Re_c \cong 430$, $\lambda \cong 2.2H$	Mode S′, (quasi-periodic), $Re_c \cong 690$,	Mode A, $Re_c \cong 700$, $\lambda \cong 3.5H$	Mode A becomes the third most unstable mode for elongated cylinders

In summary, the wakes of both compact bodies show a very similar transition scenario. The sequence of transitions is the same, with the mode shapes and structure appearing to be closely analogous. This is despite flow separation occurring from two distinct points—the leading and trailing edges—for the square cylinder, unlike the single varying separation point for each half of a circular cylinder. This naturally leads to the question of whether this state of affairs is preserved for the flow past other body shapes which possess an underlying two-dimensional quasi-periodic Kármán wake.

2.2. Normal flat plate

As for the circular cylinder there is only a single separation point on each side of the bluff body, although it is fixed in position. At low Reynolds numbers the wake resembles the typical Kármán wake of a circular cylinder. As the Reynolds number is increased the wake rapidly evolves spatially downstream to two sets of positive and negative vortices distributed on either side of the wake centreline. The two-dimensional wake as depicted by greyscale vorticity contours is shown in Fig. 3 for Reynolds numbers of 40, 80 and 130. Johnson et al. (2004) examined the two-dimensional wake state for a sequence of elliptical bodies with the circular cylinder and flat plate as limiting cases. Interestingly, the characteristic Kármán wake is displaced downstream by a wake consisting of two sets of vortices offset from the wake centreline, even at quite low Reynolds numbers, as the body geometry tends towards that of a normal flat plate. The behaviour is shown clearly in Fig. 3. Other relevant research includes Najjar and Balachandar (1997), who performed a three-dimensional numerical study of the three-dimensional wake at $\mathrm{Re} = 250$, and Julien et al. (2004, 2003) who examined the instability modes for an *idealized* wake of a normal flat plate.

Fig. 4 shows dominant Floquet multipliers against wavelength for a range of Reynolds numbers. Of the first two unstable modes, the longer wavelength mode is the first to go unstable at $\mathrm{Re} \simeq 105-110$, and has a preferred wavelength of approximately $5-6H$, where H is the height of the plate. In this case, the dominant mode has a complex multiplier (indicated by the dashed line). The shorter wavelength mode has a dominant wavelength of $\lambda/H \simeq 2$ becoming unstable at $\mathrm{Re} \simeq 125$.

Although the immediate vortex street at the rear of the body still resembles that of a circular cylinder, the mode shapes and symmetries are quite different. Fig. 5 shows perturbation spanwise vorticity contours for the shorter and

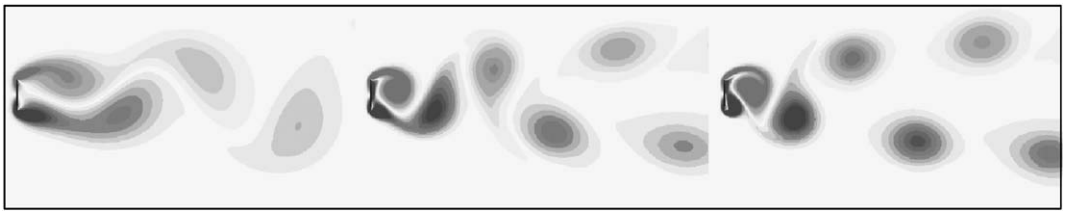

Fig. 3. Two-dimensional greyscale vorticity contours showing the shedding pattern for flow past a normal flat plate. Flow is from left to right. Left to right: $\mathrm{Re} = 40$, 80 and 130, respectively.

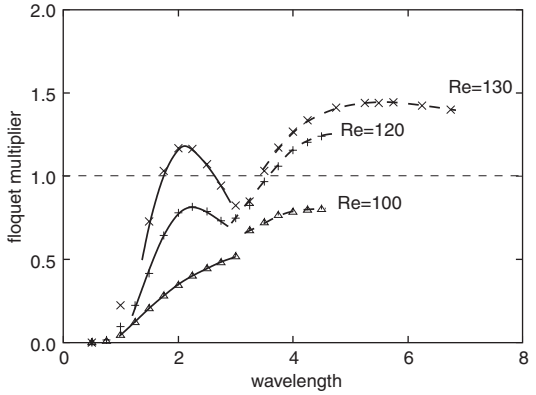

Fig. 4. Dominant Floquet multipliers for the wake of a normal flat plate.

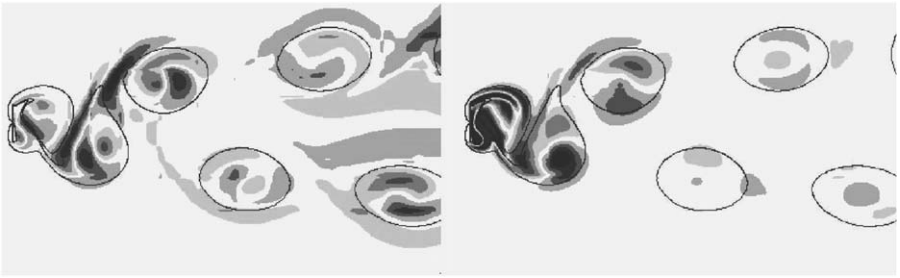

Fig. 5. Spanwise perturbation vorticity structure of the first two instability modes for the normal flat plate. The left and right images correspond to wavelengths of $\lambda/H = 2$ and 5.5, respectively. The Reynolds number is 130.

longer wavelength modes. The position of the spanwise vortex structures are indicated as well. The shorter wavelength mode has the same spatio-temporal symmetry as mode A of the circular cylinder. In addition, there is strong evidence of elliptical instability in the vortex cores, consistent with mode A (Thompson et al., 2001b). The longer wavelength mode is strong close to the rear of the plate but decays rapidly with downstream distance. As mentioned, the Floquet multiplier is complex before and after transition, and the period of the mode is not commensurate with the base flow period. Indeed, the period is highly variable with wavelength, which may indicate a rapid development to a highly chaotic wake with increasing Reynolds number.

2.3. Elongated cylinders

Results for this body geometry have been presented in Ryan et al. (2005). A summary of the key findings are presented here. Critical Reynolds numbers and wavelengths are provided in Table 1.

In this case there are three unstable modes denoted as mode A, B′ and S′, in line with the analogous modes observed for square and circular cylinders. The critical wavelengths of these modes are approximately 4, 2.2 and 1 cylinder heights, respectively. Mode A is topologically similar to, and has the same spatio-temporal symmetry of, mode A for a circular cylinder, as can be seen from the spanwise perturbation vorticity contours in Fig. 6 and isosurfaces of streamwise perturbation vorticity in Fig. 7. In particular, the sign of the perturbation vorticity is opposite on each side of the wake and this is maintained from one shedding cycle to the next (see top visualization in Fig. 7). This discounts the immediate wake where the perturbation vorticity has the opposite sign. That situation also occurs for a circular cylinder wake and has been discussed in Thompson et al. (2001b). Fig. 7 also shows Mode B′ has the same spatio-temporal symmetry as mode B of a circular cylinder with the streamwise perturbation vorticity at any spanwise position maintaining the same sign for each half-cycle; however, there are some other significant differences (hence the prime). The preferred wavelength is considerably longer ($2.2H$ compared with $0.82D$), and the perturbation field in the near wake is markedly different. Nonetheless, the downstream development is very similar. For intermediate length cylinders this mode becomes the most unstable mode, and for very long cylinders, the difference between the onset of this mode and the second mode to become unstable becomes large, as is discussed below.

Mode S′ is in some senses similar to the *almost* subharmonic mode observed by Robichaux et al. (1999). Again, the mode has a complex Floquet multiplier, although it is not close to having a subharmonic period. The real part of the Floquet multiplier only becomes greater than unity for large AR (i.e., length to height ratio) cylinders, but eventually it too becomes more unstable than mode A. For an AR of 17.5, the longest cylinder studied, mode S′ becomes unstable at $\mathrm{Re} \simeq 690$ and mode A at $\mathrm{Re} \simeq 700$. The lower visualization of Fig. 7 shows a typical snapshot of the mode S′. The mode is modulated in time.

Fig. 8 shows the variation of critical Reynolds number as a function of AR for modes A and B′. The most striking feature is that mode B′ becomes unstable at a lower Reynolds number for cylinders with AR greater than approximately 7. Indeed, for a cylinder with length to height ratio is 17.5, the difference in the critical Reynolds numbers is close to 300. Given that Karniadakis and Triantafyllou (1992) found that mode B underwent period-doubling when the existence of mode A was suppressed by artificially restricting the spanwise domain, it is not clear that the transition to turbulence will occur through the same route for elongated cylinders (or the normal flat plate) as for short cylinders. To study this aspect of transition requires full three-dimensional simulations.

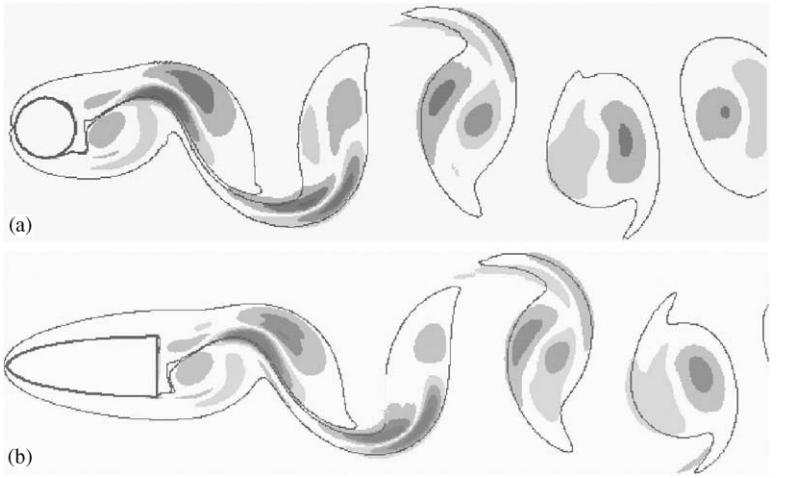

Fig. 6. Comparison of the wake spanwise vorticity field of the Floquet mode for a circular cylinder (Re = 190, $\lambda = 4D$) and short cylinder (AR = 2.5, Re = 240, $\lambda = 4H$) showing the longer wavelength instability for the short cylinder is analogous to the Mode A instability of the circular cylinder. The spatial structure of the perturbation field relative to the position of the Kármán vortices is highlighted by the contours of spanwise vorticity with $\omega_z = \pm 0.2$. Both images are at approximately the same phase in the shedding cycle. This figure corresponds to Fig. 8 of Ryan et al. (2005).

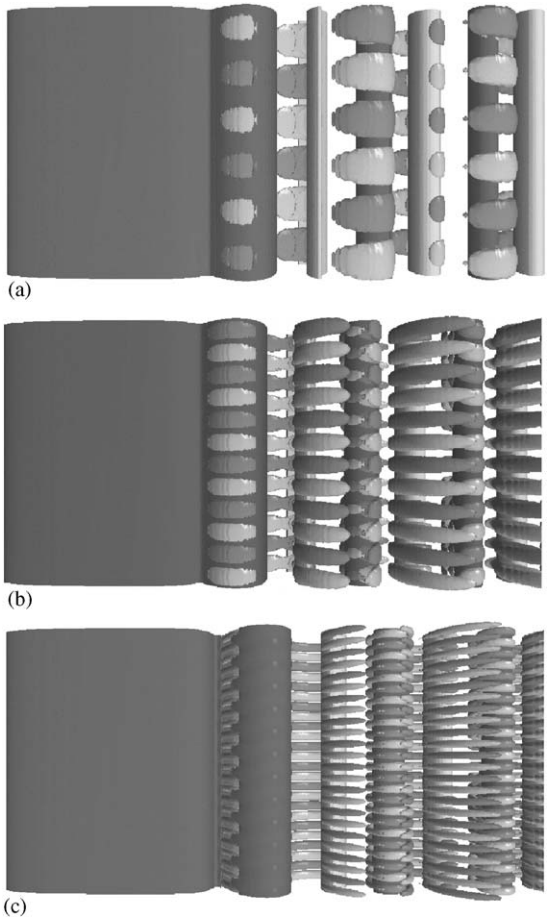

Fig. 7. Plan view of isosurfaces of the streamwise vorticity field for the three identified instability modes (A, B′ & S′) for an elliptical leading-edge cylinder. Isosurfaces of spanwise vorticity show the positions of the Kármán vortices. Note that these obscure the cylinder. The span length is $12H$. Flow is from left to right. Adapted from Figs. 17–19 of Ryan et al. (2005).

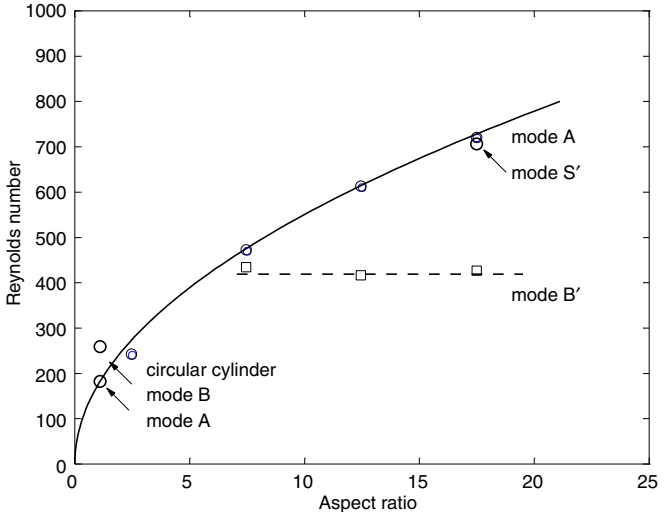

Fig. 8. Critical Reynolds number for the different mode transitions as a function of elongated cylinder aspect ratio. Here, □ indicates a Mode B′ transition and ○ indicates a Mode A transition. The curves represent an approximate fit to the data. Adapted from Fig. 12 of Ryan et al. (2005).

3. Wake transition of axisymmetric bodies

The instability modes associated with the wakes of axisymmetric bodies are discussed in this section. The generic example is flow past a sphere, and the transitions for that case have been well documented. Another interesting example is flow past a torus, which naturally transforms into a sphere, albeit topologically discontinuously, as the AR is decreased, while a section approaches the geometry of a circular cylinder as the AR becomes large. The latter was one of the reasons that this body was examined in the study of Leweke and Provansal (1995)—to remove the end effects which distort results from experimental studies of circular cylinder wakes.

Table 2 provides a summary of key findings, comparing the symmetry breaking and transition modes for a torus, and for a sphere and circular cylinder.

3.1. Sphere

This case has been studied extensively by many research groups over the years. The wake transitions not surprisingly are quite distinct from those for a circular cylinder wake. The wake undergoes a regular (i.e., time-steady) transition at $\mathrm{Re} = 212$ to the beautiful two-threaded wake (Margarvey and Bishop, 1961a,b; Johnson and Patel, 1999; Tomboulides et al., 1993, 2000; Thompson et al., 2001a; Ghidsera and Dusek, 2000; Ormières and Provansal, 1999). This wake then becomes unstable at $\mathrm{Re} \simeq 270$ through a Hopf (steady to periodic) bifurcation. At $\mathrm{Re} \simeq 350$, the vortical wake structures no longer maintain the same strict alignment from one shedding cycle to the next (Mittal, 1999). The overall wake structure is similar at considerably higher Reynolds numbers, although much more chaotic.

3.2. Torus

Sheard has undertaken an extensive numerical study of aspects of flows past tori, including three-dimensional transitions (Sheard et al., 2003b), DNS and Landau modelling, examining the saturation of the instability modes (Sheard et al., 2004), and examining wake transition to a subharmonic mode for a torus of a specific AR (Sheard et al., 2005).

Basically, the general wake behaviour naturally falls into two distinct types depending on the ratio of the ring diameter to cross-section diameter—the AR. For $\mathrm{AR} \lesssim 3.9$, the wake behaviour has strong similarities to that of a sphere, while for larger AR the torus is sufficiently large so that the local wake from sections of the torus have a lot in common with a cylinder wake. Despite the broad classification on AR, there are still considerable differences in the order in which different modes become unstable depending on AR.

Table 2
Transition behaviour for a sequence of toroidal bodies spanning the geometry of a circular cylinder to a sphere

Geometry	Geometry change relative to the circular cylinder	First instability	Second instability	Third instability	Comments
Circular cylinder	Standard case—diameter D	Mode A, $Re_c = 189$, $\lambda = 3.96D$	Mode B, $Re_c = 259$, $\lambda = 0.82D$,	Mode QP, $Re_c = 377$, $\lambda = 2D$, quasi-periodic	Saturated state has Mode B wavelength/structure at much higher Re
Torus (large diameter) AR > 3.9					
Aspect ratio: 20	Effect of slight curvature cross-section diameter = D	Mode A, $Re_c = 189$, $\lambda = 4D$	Mode B, $Re_c = 261$, $\lambda = 1D$	Mode C, $Re_c = 310$, $\lambda = 2D$	Axisymmetric geometry restricts the possible azimuthal wavelengths, corresponding to integer mode numbers
Aspect ratio: 10	Increasing curvature	Mode A, $Re_c = 194$, $\lambda = 4D$	Mode C, $Re_c = 222$, $\lambda = 2D$	Mode B, $Re_c = 270$, $\lambda = 1D$	Subharmonic mode becomes more dominant with increasing curvature, Mode B is less unstable
Aspect ratio: 5	Effect of strong curvature	Mode C, $Re_c = 164$, $\lambda = 2D$ (subharmonic)	Mode A, $Re_c = 194$, $\lambda = 4D$	Mode B, $Re_c = 310$, $\lambda = 1D$	Strong torus curvature leads to the subharmonic becoming the most unstable mode
Torus (small diameter) AR < 3.9					
Aspect ratio: 1.7–3.9	Increasing curvature	Regular (steady) non-axisymmetric transition. $Re_c = 90$ for AR = 2	Hopf bifurcation at higher Re.		
Aspect ratio: 1.6–1.7		Non-axisymmetric Hopf bifurcation			
Aspect ratio: 0–1.6	Hole disappears at AR = 1	Regular (steady) non-axisymmetric transition, $Re_c = 211$ for AR = 0, $Re_c = 73$ for	Hopf bifurcation at higher Re.		Transitions similar to a sphere prior to hole disappearing
Sphere (AR = 0)		Non-axisymmetric transition, $Re_c = 211$	Hopf bifurcation at $Re_c = 270$		

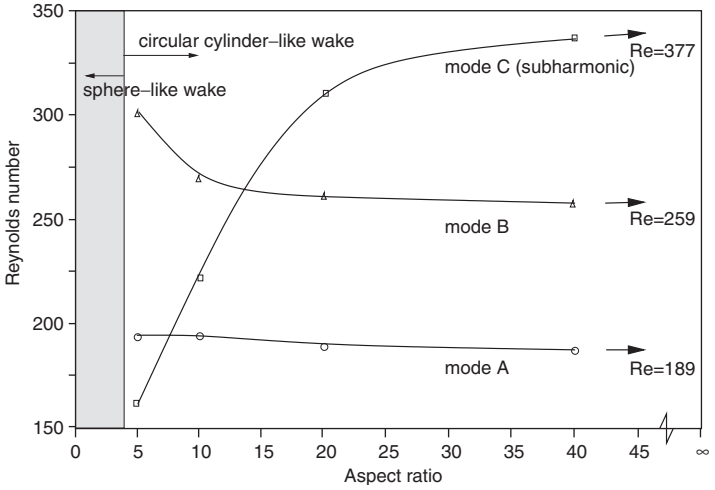

Fig. 9. Critical Reynolds number for the onset of modes A, B and C for tori for aspect ratios $AR > 5$. The critical Reynolds number for the circular cylinder wake are also provided for comparison. Adapted from Fig. 11 of Sheard et al. (2003b).

3.2.1. Small AR tori

For ARs below 1.6, the wake flow transitions are similar to those of a sphere. In particular, a regular transition occurs prior to a Hopf bifurcation. Interestingly, this Reynolds number range spans the appearance of the *hole* in the toriodal geometry at AR = 1, yet the wake behaviour is continuous across this topology change. For $1.6 < \mathrm{AR} < 1.7$, the axisymmetric steady wake undergoes a Hopf bifurcation with azimuthal mode number $m = 1$, in the absence of any regular bifurcation. At larger ARs, $1.7 \lesssim \mathrm{AR} \lesssim 3.9$, again the regular bifurcation occurs first.

3.2.2. Large AR tori

For large ARs, the analogues of modes A and B of the cylinder wake also occur for this geometry, with similar preferred wavelengths but restricted by the discreteness of mode selection due to the periodic azimuthal geometry. For each mode, the spatio-temporal symmetry is approximately preserved, together with the general mode shape, i.e., the spatial distribution of the perturbation field. The curvature does result in a clearly observable loss of symmetry between the two sides of the wake. Importantly, even for large AR tori, the small ring curvature still leads to a noticeable loss of the symmetry that is clearly visible in the plane defined by the flow direction and cylinder axis for a two-dimensional cylinder. This change to symmetry group properties allows a true subharmonic mode to develop (mode C), which is in fact the first occurring instability mode for tori of ARs $4 \lesssim \mathrm{AR} \lesssim 8$. Fig. 9 shows the transition Reynolds numbers for modes A, B and C, for AR = 5. Sheard et al. (2005) provide experimental verification of this transition sequence for moderate AR tori.

DNS using restricted spanwise arcs based on the preferred wavelengths determined from the Floquet instability analysis have been used to examine the saturated states. Fig. 10 shows visualizations of these three modes for a torus of AR = 10. The spatio-temporal symmetry displayed by each mode can be observed from these plots.

4. Physical mechanisms of transition

There has been a debate over the physical mechanisms responsible for the development of these instabilities. There have been suggestions that mode A is due to a Benjamin–Feir instability (Leweke and Provansal, 1995), a centrifugal instability of the braid region between the main vortex rollers (Brede et al., 1996), and an elliptical instability of the vortex cores (Leweke and Williamson, 1998b; Thompson et al., 2001b). Speculation has also occurred for mode B, certainly in terms of a three-dimensional shear layer instability of the separating shear layers (Brede et al., 1996), a centrifugal instability (Ryan et al., 2005) and a hyperbolic instability of the braid region (Leweke and Williamson, 1998b). Naturally, the flow field is complex and hence it is not clear that the development of an instability can be entirely attributed to a unique physical instability mechanism that governs a very simple flow topology. Nevertheless, it is appealing to do this to provide some physical insight into the evolution of the flow as the Reynolds number is increased.

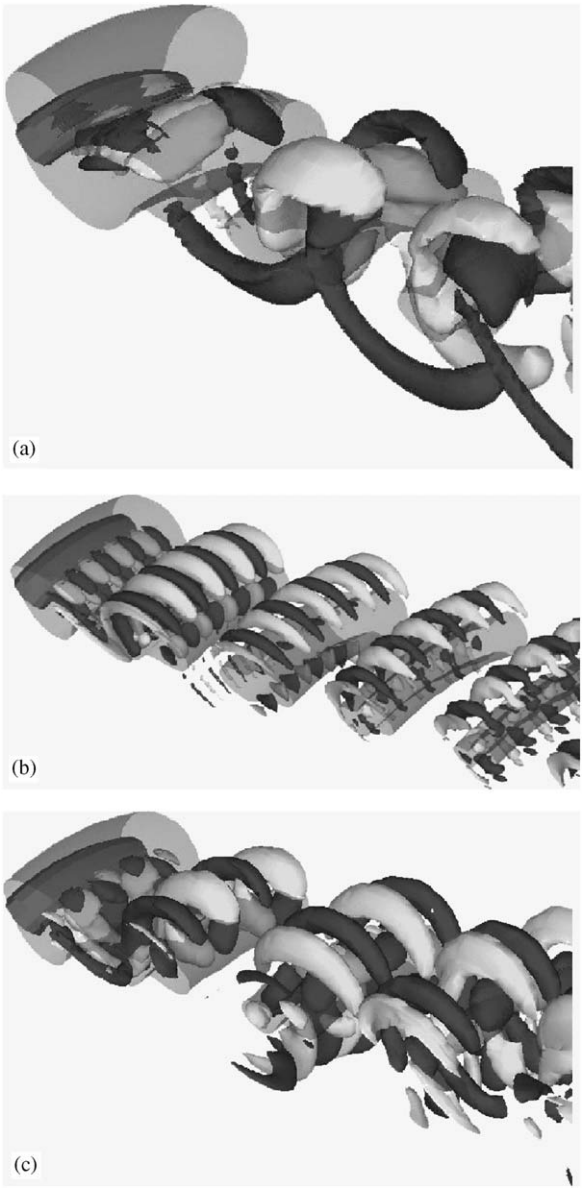

Fig. 10. Perspective view of the three saturated instability modes for a large aspect ratio torus. In this case, AR = 10. The flow is visualized using isosurfaces of positive and negative streamwise vorticity, which reveals the spatio-temporal symmetry. Top to bottom: mode A (Re = 200), mode B (Re = 280) and mode C (Re = 235), respectively. Semi-transparent isosurfaces showing sections of the torus and the positions of the axi-symmetric rollers are also provided. Flow is from top left to bottom right. Adapted from Fig. 23 of Sheard et al. (2004).

For mode A, it appears that the elliptical instability mechanism strongly contributes to the development of the instability. Williamson (1996a,b) suggested that for a circular cylinder, the instability modes scale with the wake vortex cores (mode A) and the width of the braids between the cores (mode B). Leweke and Williamson (1998b) explored the possibility that mode A was primarily elliptic in origin by analytically calculating the growth rate of the strained vortex cores to an elliptic instability. The growth over a cycle was found to be substantial, and it was speculated that this would provide sufficient feedback from one shedding cycle to the next to sustain the instability. In addition, the analytically predicted spanwise wavelength for an elliptic instability closely matched the experimentally observed and numerically

predicted wavelength. Thompson et al. (2001b) examined the growth of the mode through DNS. These authors showed that as each pair of wake vortices form and begin to shed, the perturbation fields within the cores are locally consistent with the signature of elliptic instability. Effectively, a cooperative elliptic instability (Leweke and Williamson, 1998a) develops between the shedding vortices. However, the perturbation then grows rapidly between the cores, where the flow is undergoing rapid straining. DNS established that the mode A field would recover more quickly if the perturbation field was artificially zeroed in the parts of the domain where the flow was hyperbolic rather than elliptic. It appears that the instability is slaved to the elliptic core instability. Julien et al. (2004) found similar behaviour occurring between vortex cores for Bickley flow as an idealized model of the wake from a normal flat plate. Again, the core instability controls the wavelength and overall growth rate although the perturbation field appears strong between the cores.

Mode B shows strong growth in the braids and between the forming Kármán vortices. The development of the perturbation field within the vortex cores is much reduced and does not show a strong signature of an elliptic instability. Indeed, the preferred wavelength is probably too small for amplification through an elliptic mechanism. In Ryan et al. (2005) an attempt is made to associate the instability with a centrifugal instability. The spatio-temporal topology of the mode is consistent with a centrifugal instability, in that the streamwise vortices identified with the development of the perturbation extend downstream as unbroken tubes along the braids. This provides a feedback mechanism from one cycle to the next, sustaining the perturbation. An idealized stability analysis, based on isolating part of the near wake region where the growth rate is large, shows that the predicted instability wavelength is within 25% of the preferred wavelength of mode B. In addition, the predicted growth rate applicable to the time taken for fluid parcels to travel through this region on circular streamlines is also within 30% of the total growth measured directly from DNS for the corresponding time.

5. Conclusion

The sequence of three-dimensional modes involved in the wake transition from two-dimensional (or axisymmetric) flow to three-dimensional flow is very much a function of bluff body geometry. For example, for elongated cylinders with a blunt trailing edge, an analogue of mode B for the circular cylinder wake becomes unstable at a much lower Reynolds number than mode A. As the AR increases, the difference in critical Reynolds number becomes large. However, while this mode has the same spatio-temporal symmetry as mode B, its perturbation field structure is considerably different in the near wake, and the preferred spanwise wavelength is 2.5 times greater. For a torus, for intermediate ARs $4 \lesssim AR \lesssim 8$, mode C, which is subharmonic and at least superficially appears related to the almost subharmonic mode occurring in a circular cylinder wake, is the most unstable mode. On the other hand, for a normal flat plate, the most unstable mode is a long wavelength quasiperiodic mode—which does not appear to be closely related to any of the circular cylinder wake modes.

Whether the different transition sequences and existence of different modes significantly alters the transition to a chaotic flow state, or affects the final turbulent state at higher Reynolds numbers, are still open questions. This will require full direct simulations and careful experiments, which are currently underway.

The association of complex three-dimensional instability modes with generic physical instability mechanisms is also considered briefly in this article. There does seem to be reasonable circumstantial evidence supporting this interpretation, including the prediction of instability wavelengths and growth rates. There is also evidence that multiple mechanisms may contribute. For example, for mode B, the characteristic signature of the elliptical instability can be seen in the cores of the Kármán rollers downstream, yet the maximum perturbation amplitude appears to develop in the forming braids between the rollers in the near wake, and this shows hallmarks of being driven by a centrifugal instability. In addition, for mode A, the elliptic instability mechanism appears to act separately in the near wake and further downstream.

References

Barkley, D., Henderson, R.D., 1996. Three-dimensional Floquet stability analysis of the wake of a circular cylinder. Journal of Fluid Mechanics 322, 215–241.

Bays-Muchmore, B., Ahmed, A., 1993. On streamwise vortices in turbulent wakes of a cylinder. Physics of Fluids A 5 (2), 387–392.

Blackburn, H.M., Lopez, J.M., 2003. On three-dimensional quasiperiodic Floquet instabilities of two-dimensional bluff body wakes. Physics of Fluids 15, L57–L60.

Blackburn, H.M., Marques, F., Lopez, J.M., 2005. Symmetry breaking of two-dimensional time-periodic wakes. Journal of Fluid Mechanics 552, 395–411.

Brede, M., Eckelmann, H., Rockwell, D., 1996. On secondary vortices in a cylinder wake. Physics of Fluids 8, 2117–2124.

Gerrard, J.H., 1978. The wakes of cylindrical bluff bodies at low Reynolds numbers. Philosophical Transactions of the Royal Society of London, Series A 288, 351–382.

Ghidsera, B., Dusek, J., 2000. Breaking of axisymmetry and onset of unsteadiness in the wake of a sphere. Journal of Fluid Mechanics 423, 33–69.

Henderson, R., 1997. Nonlinear dynamics and pattern formation in turbulent wake transition. Journal of Fluid Mechanics 352, 65–112.

Johnson, T.A., Patel, V.C., 1999. Flow past a sphere up to a Reynolds number of 300. Journal of Fluid Mechanics 378, 19–70.

Johnson, S.A., Thompson, M.C., Hourigan, K., 2004. Predicted low frequency structures in the wake of elliptical cylinders. European Journal of Mechanics B/Fluids 23 (1), 229–239.

Julien, S., Lasheras, J., Chomaz, J., 2003. Three-dimensional instability and vorticity patterns in the wake of a flat plate. Journal of Fluid Mechanics 479, 155–189.

Julien, S., Ortiz, S., Chomaz, J.-M., 2004. Secondary instability mechanisms in the wake of a flat plate. European Journal of Mechanics B/Fluids 23 (1), 157–165.

Karniadakis, G.E., Triantafyllou, G.S., 1992. Three-dimensional dynamics and transition to turbulence in the wake of bluff objects. Journal of Fluid Mechanics 238, 1–30.

Leweke, T., Provansal, M., 1995. The flow behind rings: bluff body wakes without end effects. Journal of Fluid Mechanics 288, 265–310.

Leweke, T., Williamson, C.H.K., 1998a. Cooperative elliptic instability of a vortex pair. Journal of Fluid Mechanics 360, 85–119.

Leweke, T., Williamson, C.H.K., 1998b. Three-dimensional instabilities in wake transition. European Journal of Mechanics B/Fluids 17, 571–586.

Margarvey, R.H., Bishop, R.L., 1961a. Transition ranges for three-dimensional wakes. Canadian Journal of Physics 39, 1418–1422.

Margarvey, R.H., Bishop, R.L., 1961b. Wakes in liquid-liquid systems. Physics of Fluids 4 (7), 800–805.

Miller, G.D., Williamson, C.H.K., 1994. Control of three-dimensional phase dynamic in a cylinder wake. Experiments in Fluids 18, 26.

Mittal, R., 1999. Planar symmetry in the unsteady wake of a sphere. AIAA Journal 37 (3), TN388–TN390.

Mittal, R., Balachandar, S., 1995. Generation of streamwise structures in bluff body wakes. Physical Review Letters 75, 1300.

Najjar, F.M., Balachandar, S., 1997. Low-frequency unsteadiness in the wake of a normal flat plate. Journal of Fluid Mechanics 370, 101–147.

Ormières, D., Provansal, M., 1999. Transition to turbulence in the wake of a sphere. Physical Review Letters 83, 80–83.

Robichaux, J., Balachandar, S., Vanka, S.P., 1999. Three-dimensional Floquet instability of the wake of square cylinder. Physics of Fluids 11, 560–578.

Ryan, K., Thompson, M.C., Hourigan, K., 2005. Three-dimensional transition in the wake of elongated bluff bodies. Journal of Fluid Mechanics 538, 1–29.

Sheard, G.J., Thompson, M.C., Hourigan, K., 2003a. A coupled Landau model describing the Strouhal–Reynolds number profile of a three-dimensional circular cylinder wake. Physics of Fluids Letters 15 (9), 68–71.

Sheard, G.J., Thompson, M.C., Hourigan, K., 2003b. From spheres to circular cylinders: the stability and flow structures of bluff ring wakes. Journal of Fluid Mechanics 492, 147–180.

Sheard, G.J., Thompson, M.C., Hourigan, K., 2004. From spheres to circular cylinders: non-axisymmetric transition in the flow past rings. Journal of Fluid Mechanics 506, 45–78.

Sheard, G.J., Thompson, M.C., Hourigan, K., Leweke, T., 2005. The evolution of a subharmonic mode in a vortex street. Journal of Fluid Mechanics 534, 23–38.

Thompson, M.C., Hourigan, K., Sheridan, J., 1994. Three-dimensional instabilities in the cylinder wake. In: Hourigan, K., Shepherd, I. (Eds.), International Colloquium on Jets, Wakes and Shear Layers, CSIRO, DBCE, Highett. Melbourne, Australia, April 18–20.

Thompson, M.C., Hourigan, K., Sheridan, J., 1996. Three-dimensional instabilities in the wake of a circular cylinder. Experimental and Thermal Fluid Science 12, 190–196.

Thompson, M.C., Leweke, T., Provansal, M., 2001a. Kinematics and dynamics of sphere wake transition. Journal of Fluids and Structures 15, 575–585.

Thompson, M.C., Leweke, T., Williamson, C.H.K., 2001b. The physical mechanism of transition in bluff body wakes. Journal of Fluids and Structures 15, 607–616.

Tomboulides, A.G., Orzsag, S.A., Karniadakis, G.E., 1993. Direct and large eddy simulations of axisymmetric wakes. AIAA paper 93-0546.

Tomboulides, A.G., Orzsag, S.A., Karniadakis, G.E., 2000. Numerical investigation of transitional and weak turbulent flow past a sphere. Journal of Fluid Mechanics 416, 45–73.

Williamson, C.H.K., 1988a. Defining a universal and continuous Strouhal–Reynolds number relationship for the laminar vortex shedding of a circular cylinder. Physics of Fluids 31, 2742–2744.

Williamson, C.H.K., 1988b. The existence of two stages in the transition to three dimensionality of a cylinder wake. Physics of Fluids 31, 3165–3168.

Williamson, C.H.K., 1996a. Three-dimensional wake transition. Journal of Fluid Mechanics 328, 345–407.

Williamson, C.H.K., 1996b. Vortex dynamics in the cylinder wake. Annual Reviews of Fluid Mechanics 28, 477–539.
Wu, J., Sheridan, J., Welsh, M.C., Hourigan, K., 1996. Three-dimensional vortex structures in a cylinder wake. Journal of Fluid Mechanics 312, 201–222.
Zhang, H., Fey, U., Noack, B.R., Koenig, M., Eckelmann, H., 1995. On the transition of the cylinder wake. Physics of Fluids 7, 779–794.